European Spine Journal (2020) 29:3187–3193
https://doi.org/10.1007/s00586-020-06632-z

ORIGINAL ARTICLE

# Differentiating atypical hemangiomas and vertebral metastases: a field-of-view (FOV) and FOCUS intravoxel incoherent motion (IVIM) diffusion-weighted imaging (DWI) study

**Jibin Cao[1] · Sijia Gao[1] · Chenying Zhang[1] · Yinxia Zhang[2] · Wenge Sun[1] · Lingling Cui[1]**

Received: 1 July 2020 / Revised: 15 September 2020 / Accepted: 7 October 2020 / Published online: 19 October 2020


## Abstract

**Purpose** Some atypical vertebral hemangiomas (VHs) may mimic metastases on routine MRI and can result in misdiagnosis and ultimately to additional imaging, biopsy and unnecessary costs. The purpose of this study is to assess the utility of intravoxel incoherent motion (IVIM) diffusion-weighted imaging (DWI) on account of field-of-view optimized and constrained undistorted single shot (FOCUS) in distinguishing atypical VHs and vertebral metastases.

**Methods** A total of 25 patients with vertebral metastases and 25 patients with atypical VHs were confirmed by clinical follow-up or pathology. IVIM-DWI imaging was performed at different *b* values (0, 30, 50, 100, 150, 200, 400, 600, 800, 1000 $mm^2/s$). IVIM parameters [the true diffusion coefficient (*D*), pseudodiffusion coefficient (*D**), standard apparent diffusion coefficient (ADC), and perfusion fraction (*f*)] were calculated and compared between two groups by using Student's *t* test. A receiver operating characteristic analysis was performed.

**Results** Quantitative analysis of standard ADC and *D* parameters showed significantly lower values in vertebral metastases when compared to atypical hemangiomas [ADC value: $(0.70 \pm 0.12) \times 10^{-3}$ $mm^2/s$ vs $(1.14 \pm 0.28) \times 10^{-3}$ $mm^2/s$; *D* value: $(0.47 \pm 0.07) \times 10^{-3}$ $mm^2/s$ vs $(0.76 \pm 0.14) \times 10^{-3}$ $mm^2/s$, all $P < 0.01$]. The sensitivity and specificity of *D* value were 93.8% and 92.3%, respectively.

**Conclusion** The standard ADC value and *D* value may be used as an indicator to distinguish vertebral metastases from atypical VHs. FOCUS IVIM-derived parameters provide potential value in the quantitatively differentiating vertebral metastases from vertebral atypical hemangiomas.

**Keywords** Intravoxel incoherent motion · IVIM · Diffusion magnetic resonance imaging · DWI · Vertebral metastases

✉ Lingling Cui
cmu00ring@163.com

Jibin Cao
cmucao@163.com

Sijia Gao
cmugao@163.com

Chenying Zhang
1924931552@qq.com

Yinxia Zhang
397517044@qq.com

Wenge Sun
wengesun@sina.com

[1] Department of Radiology, The First Hospital of China Medical University, 155 Nanjing North Street, Heping District, Shenyang 110001, Liaoning, People's Republic of China

[2] Department of Radiology, Zhengzhou University Affiliated Zhengzhou Central Hospital, Zhengzhou, China

## Introduction

It is reported that vertebral metastases occur in 5–10% of patients with primary tumors [1]. To detect or exclude vertebral metastases is clinically vital to provide staging information and guide treatment regimen and prognosis for patients with malignant tumor [2]. Vertebral hemangiomas (VHs) are common benign bone tumors that are always incidentally reported in 11% of spines in the adult autopsy series [3–5]. They usually have a typical radiographic appearance with hyperintense on T1- and T2-weighted images in relation to the surrounding normal vertebral bone marrow [6]. Occasionally, some atypical VHs may show similar metastatic findings on conventional magnetic resonance imaging (MRI) with hypo- or isointense on T1-weighted images [7, 8]. When the atypical VHs mimic vertebral metastases, the radiologic differential diagnosis is challenging. Therefore,

it is very important to distinguish vertebral metastases from atypical VHs in cancer patients clinically [9, 10].

In recent years, intravoxel incoherent motion (IVIM) diffusion-weighted imaging (DWI) allows evaluating angiogenesis or microvascular heterogeneity based on the perfusion information without using contrast agent [11–13] and has become an effective method to diagnose disease in different organs [14–17]. The parameters for the true diffusion coefficient (*D*), pseudodiffusion coefficient (*D**) and microperfusion fraction (*f*) related to the vascularity can be calculated by using IVIM [18–20]. IVIM can separate perfusion (or microcirculation)-related diffusion from pure molecular diffusion, by analyzing the signal attenuation of multi-b-value DWI [15, 17]. High *b* value reflects the diffusion characteristics of water molecules, while low *b* value reflects the perfusion characteristics of tissues [21]. IVIM parameters measurement has recently been confirmed in the spine of healthy volunteers [20].

A more detailed description of the signal attenuation may provide more complex information about pathologic changes in living tissue [18, 19]. The field-of-view (FOV) optimized and constrained undistorted single shot (FOCUS), a new diffusion technique, allows for a FOV reduction in the phase-encode direction, which allows reducing the readout duration required for ss-EPI, resulting in better diffusion images and better anatomical details [22].

To the best of our knowledge, the feasibility studies of IVIM in vertebral lesions are limited [23, 24]. Therefore, the purpose of our study was to evaluate the application of FOCUS IVIM-DWI in identifying atypical VHs and vertebral metastases. We suggest that the IVIM technology can accurately identify two diseases at an early stage, which is conducive to the clinical treatment plan and the improvement of prognosis.

## Material and methods

### Participants

Consecutive subjects were sought from January 2018 to 2020. The inclusion criteria for patients were the following: (1) a history of primary malignancy confirmed by needle biopsy or pathological examination; (2) patients with spinal lesions who undergone conventional MR and IVIM imaging, and ≥ 6-month follow-up with either MR or CT imaging; and (3) no radiation and chemotherapy history. Exclusion criteria were the following: (1) lesions without a complete MRI examination; (2) spinal lesions complicated with fracture; and (3) lesions of osteoblastic metastases. This study was approved by Ethics Committee of our hospital, and informed consent was obtained.

### MR acquisition protocols

All measurements on patients were performed on a GE Signa HDX 3.0 T MRI scanner (General Electric, USA) equipped with an 8-channel phased array spine coil in supine position. All patients underwent routine MRI, including sagittal T1-weighted fast spine echo (FSE) sequence: repetition time (TR) = 560 ms; echo time (TE) = Min Full; slice thickness = 4 mm; gap = 1.0 mm; field of view (FOV) = 320 × 320 mm; matrix = 320 × 192; number of excitations (NEX) = 4, T2 weighted FSE sequence: TR = 2500 ms; TE = 120 ms; slice thickness = 4 mm; gap = 1.0 mm; FOV = 200 × 200 mm; matrix = 288 × 256; NEX = 2, and sagittal T2 weighted fat suppression (FS) sequence: TR = 3200 ms; TE = 85 ms; slice thickness = 4 mm; gap = 1.0 mm; FOV = 320 × 320 mm; matrix = 352 × 256, NEX = 2.

Axial DW images were obtained by using single-shot spin-echo echo-planar imaging (EPI) sequences: TR = 3200 ms; TE = 81 ms; slice thickness = 4 mm; spacing = 0.5 mm; FOV = 200 × 200 mm; matrix = 160 × 160; and NEX = 2. The sequence worked with spectral presaturation inversion recovery (SPIR) and diffusion sensitization in the anterior–posterior direction applied with weighting factors of *b* 0, 30, 50, 100, 150, 200, 400, 600, 800 and 1000 s/mm$^2$. Total scan time for the IVIM scan was 260 s.

### Image post-processing and regions of interest (ROI)

Two radiologists manually located all areas of interest (ROIs) on an image with a *b* value = 0 s/mm$^2$ and then copied them to the corresponding *D*, *D**, ADC and *f* maps. In each patient, plane that could display the largest lesions was chosen for the ROI measurement. All ROIs were kept away from necrotic, hemorrhages, cysts and other areas of fluid collections in the lesions. Four circular ROIs were manually drawn in each patient image (Figs. 1, 2). The values of the 4 ROIs were used for the final analysis.

### 2.4. Reference standards

Two radiologists with 5 years and 8 years of experience in spinal MR imaging reviewed available clinical information in all selected patients with spinal lesions, including the demographic data, tumor history and the imaging results. The investigators described the MRI and CT findings of each spinal lesion (hemangioma or metastases) and the changes in the size and number of lesions after more than 6-month follow-up [4, 25]. Based on the previous studies,

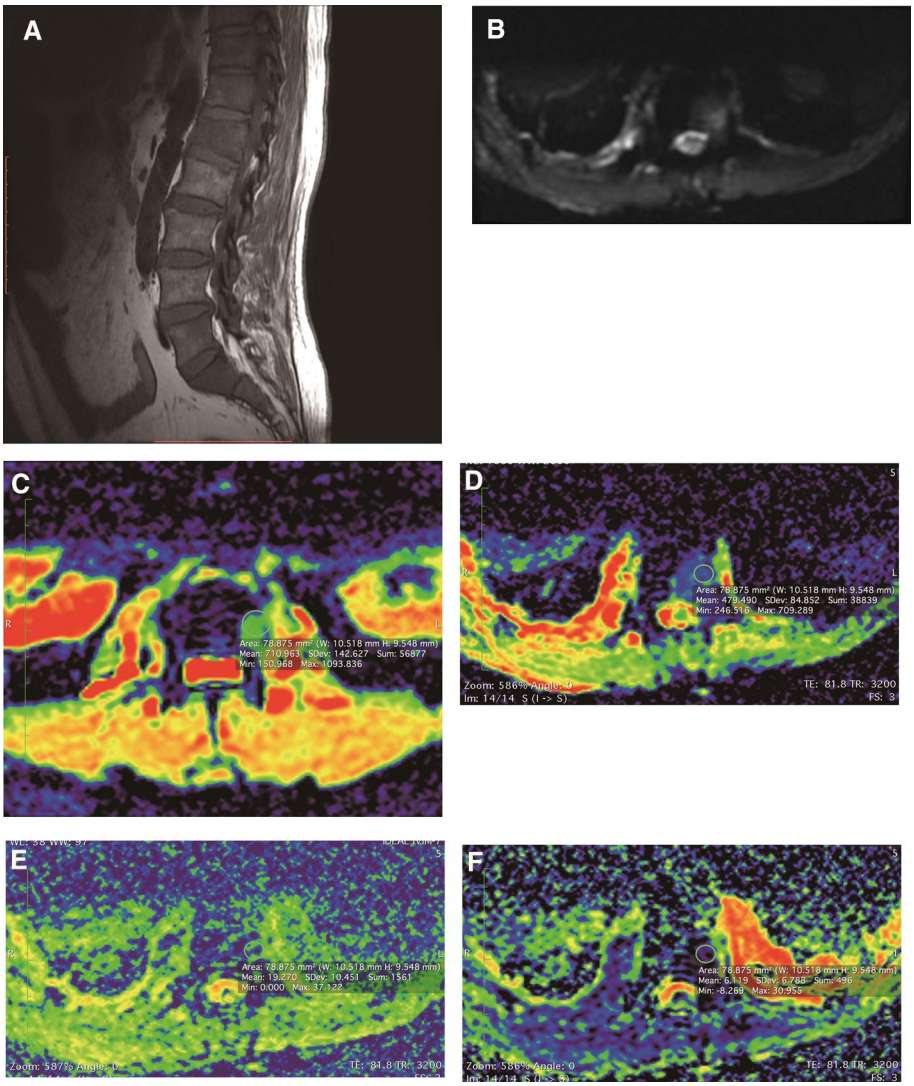


**Fig. 1** **a**, **b** A 63-year-old man with a remote history of breast cancer and metronomics chemotherapy. The vertebral metastases are identified with a focal area of hypointensity at T11-L1, L5-S2 on the sagittal T1-weighted image (**a**), hyperintense signal in diffusion-weighting imaging (**b**); **c**–**f** plane that displays the largest lesions at L1 was chosen for the ROI measurement. The ADC value (**c**), *D* value (**d**), *D** value (**e**) and *f* value (**f**) of lesion were $0.71 \times 10^{-3}$ mm$^2$/s, $0.48 \times 10^{-3}$ mm$^2$/s, $1.93 \times 10^{-3}$ mm$^2$/s and 6.12%, respectively

more than 6-month follow-up using radiological imaging examination to describe the lesions was one of the criterions [5, 26, 27].

VH was diagnosed by histological examination result (if any) or radiological imaging revealing characteristic trabecular appearance based on follow-up showing radiological and clinical stability at least 6 months [25]. Atypical hemangioma is hemangioma with iso- or hypointense on T1-weighted images [7, 8]. Spinal metastases were diagnosed by history (if any) or radiological imaging showing osteolytic changes of metastatic lesions or follow-up showing radiological and clinical progression or therapeutic response after at least 6-month anticancer treatment.

## Data analysis

Mean values of *D*, *D**, ADC and *f* were tested for significant differences between tumor tissue and control region of each patient using a Student's *t* test. Mann–Whitney *U*-test was used to compare the differences of each parameter between two groups. The data were analyzed using SPSS 19.0 software (SPSS, Chicago, IL, USA), and $P < 0.05$ was considered statistically significant. The univariate receiver operating characteristic curve (ROC) analyses were performed, and areas under the curve (AUC) were compared to indicate the accurateness of the different parameters. We established optimal thresholds and corresponding sensitivities and specificities.

## Results

Twenty-five consecutive patients with atypical VHs including 32 lesions (11 males, 14 females; mean age $56.74 \pm 9.45$ years; age range 35–68 years) and 25 consecutive patients with vertebral metastases including 52 metastatic lesions (12 males, 13 females; mean age

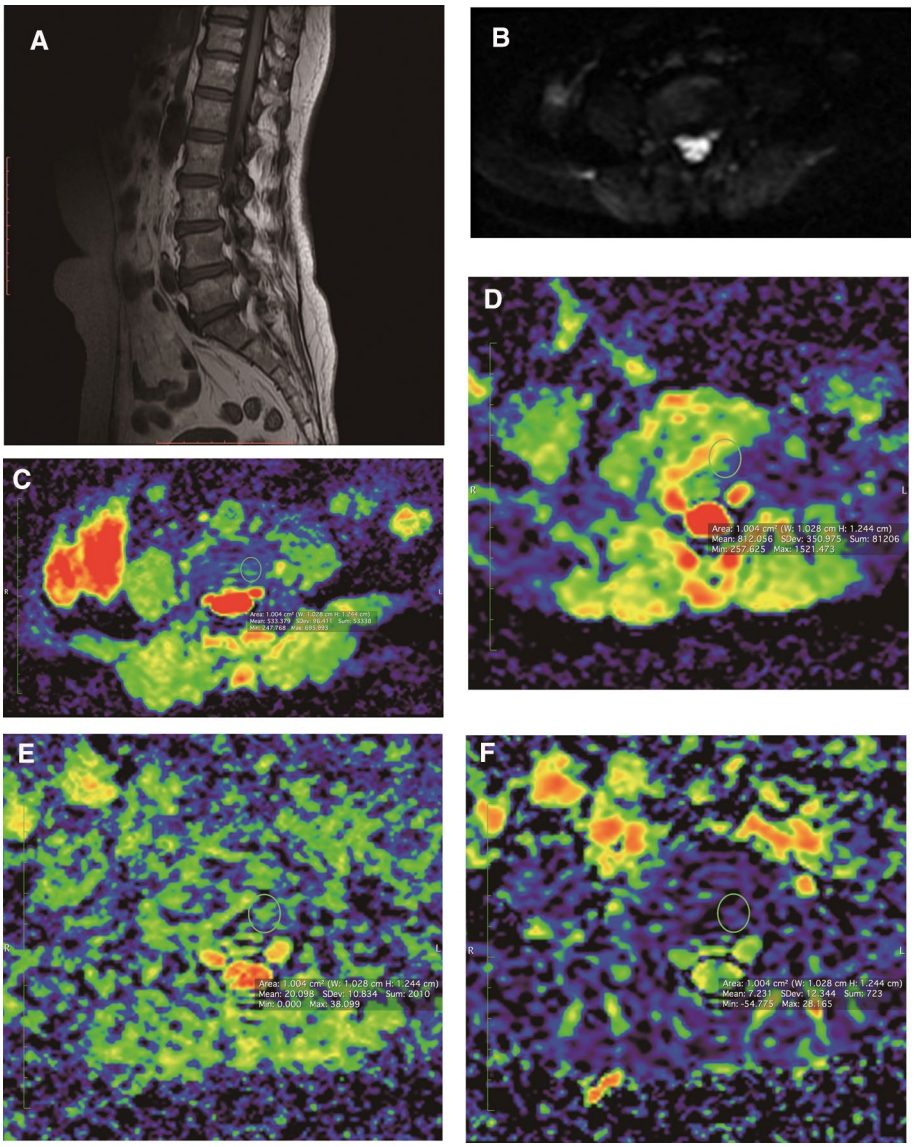


**Fig. 2** **a**, **b** A 43-year-old man with a remote history of breast cancer. The atypical hemangioma is identified by histological examination with a focal area of hypointensity at L4 on the sagittal T1-weighted image. **a**, hypointense signal in diffusion-weighting imaging (**b**); **c**–**f** plane that displays the largest lesions was chosen for the ROI measurement. The ADC value (**c**), *D* value (**d**), *D** value (**e**) and *f* value (**f**) of lesion were $0.53\times10^{-3}$ mm$^2$/s, $0.81\times10^{-3}$ mm$^2$/s, $2.01\times10^{-3}$mm$^2$/s and 7.23%, respectively

61.48 ± 1.05 years; age range 45–65 years) were recruited from our clinics.

Quantitative analysis of standard ADC and *D* parameters showed significantly lower values in vertebral metastases when compared to atypical VHs [ADC value: $(0.70\pm0.12)\times10^{-3}$ mm$^2$/s vs $(1.14\pm0.28)\times10^{-3}$ mm$^2$/s; *D* value: $(0.47\pm0.07)\times10^{-3}$ mm$^2$/s vs $(0.76\pm0.14)\times10^{-3}$ mm$^2$/s, all $P<0.01$]. There was no statistically significant difference in *D** and *f* values between vertebral metastases and atypical VHs [*D** value: $(1.31\pm0.62)\times10^{-3}$ mm$^2$/s vs $(1.43\pm0.94)\times10^{-3}$ mm$^2$/s; *f* value: $(0.45\pm0.25)\times10^{-3}$mm$^2$/s vs $(0.52\pm0.20)\times10^{-3}$mm$^2$/s, all $P>0.05$] (Table1, Fig. 3).

The AUC of ADC value and standard *D* value were AUC = 0.911, 95%CI: 0.829–0.993, $P<0.01$ and AUC = 0.978, 95%CI: 0.829–1.000, $P<0.01$, respectively.

**Table 1** IVIM-DWI parameter values in vertebral metastases and atypical VHs group

| Parameter values | Vertebral metastases | Atypical VHs | *P* value |
|---|---|---|---|
| ADC ($\times10^{-3}$ s/mm$^2$) | 0.70 ± 0.12 | 1.14 ± 0.28 | < 0.01 |
| *D* ($\times10^{-3}$ s/mm$^2$) | 0.47 ± 0.07 | 0.76 ± 0.14 | < 0.01 |
| *D** ($\times10^{-3}$ s/mm$^2$) | 1.31 ± 0.62 | 1.43 ± 0.94 | 0.731 |
| *F*(%) | 0.45 ± 0.25 | 0.52 ± 0.20 | 0.340 |

The sensitivity and specificity of standard ADC value were 87.5%, 88.5%, and those of *D* value were 93.8%, 92.3%, respectively (Fig. 4). The cutoff value of *D* value was $0.575\times10^{-3}$ mm$^2$/s, indicating that when *D* value was less than $0.575\times10^{-3}$ mm$^2$/s, lesions could be diagnosed as vertebral metastases.

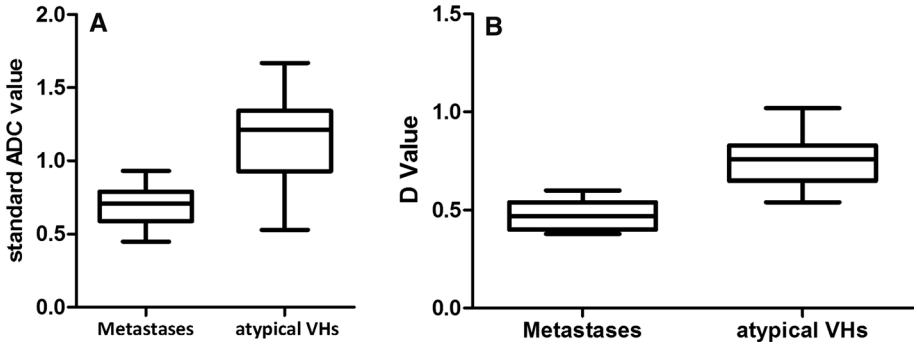


**Fig. 3** Quantitative analysis of standard ADC (**a**) and *D* (**b**) parameters showed significantly lower values in vertebral metastases when compared to atypical VHs [ADC value: $(0.70 \pm 0.12) \times 10^{-3}$ mm$^2$/s vs $(1.14 \pm 0.28) \times 10^{-3}$mm$^2$/s; *D* value: $(0.47 \pm 0.07) \times 10^{-3}$mm$^2$/s vs $(0.76 \pm 0.14) \times 10^{-3}$mm$^2$/s, all $P < 0.01$]

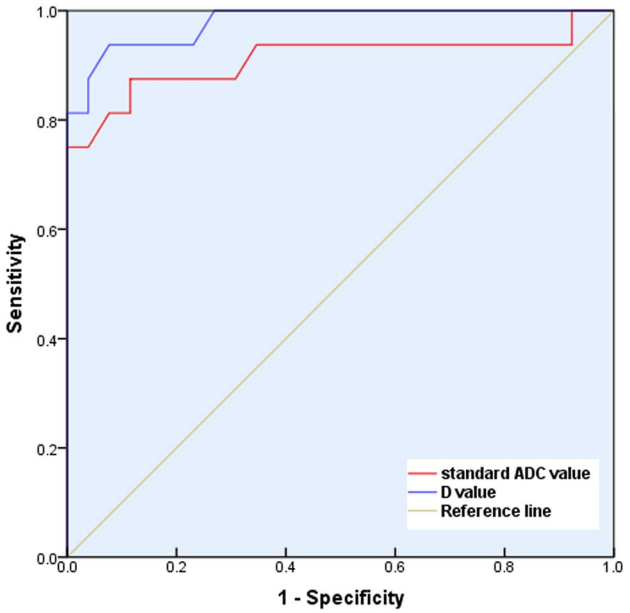


**Fig. 4** The AUC of ADC value and standard *D* value were AUC = 0.911, 95%CI: 0.829–0.993, $P < 0.01$ and AUC = 0.978, 95%CI: 0.829–1.000, $P < 0.01$, respectively. The sensitivity and specificity of standard ADC value were 87.5%, 88.5%, and those of *D* value were 93.8%, 92.3%, respectively

## Discussion

Our objective is to assess the utility of FOCUS IVIM in distinguishing atypical VHs and vertebral metastases. The standard ADC value and *D* value may be used as an indicator to distinguish vertebral metastases from atypical VHs. We confirmed the feasibility of FOCUS IVIM technique to acquire a higher-resolution DW images in vertebral bone marrow and distinguish the atypical VHs and vertebral metastases in our study.

The feasibility of a bi-exponential approach in DW imaging represents a technical challenge. The FOCUS technique has been performed for DWI of the lumbar nerve roots, pancreas, breast and prostate gland [28–31]. These studies confirmed that FOCUS DWI is an optimized sequence that can better promote spatially selective excitation and improve image quality due to a less deformation and a higher spatial resolution. This may improve the accuracy of DWI in detecting lesions, especially for the small lesions. In our study, we examine the diagnostic capacity of IVIM parameters of spinal lesions.

Previous studies on vertebral bone marrow have reported that in [32, 33], the standard ADC values and *D* values corresponding to water molecular diffusion and perfusion in normal vertebral bodies were very low, ranging from 0.2 to $0.6 \times 10^{-3}$ mm$^2$/s and 0.1 to $0.3 \times 10^{-3}$ mm$^2$/s. Our results were similar to most previous studies [13, 34, 35]. We suggested that the ADC value and *D* value were increased in the vertebral lesions (both benign and malignant), which is more sensitive than the conventional DWI in detecting the water molecular diffusion changes. When vertebral lesions occur, the bone marrow is invaded, and the fat within the bone marrow is replaced by the lesions, leading to increased water content and the blood perfusion. Thus, the diffusion ability of bone marrow may increase, and the corresponding standard ADC value and *D* value also increase [33, 34]. IVIM-DWI may be an effective method and more accurate for the quantitative diagnosis of vertebral lesions at the molecular level [36].

We have found that the standard ADC value and *D* value of vertebral metastases in this study were lower than that of atypical VHs. This is basically consistent with most previous studies [37, 38]. When the neoplastic lesion infiltrates into the vertebral bone marrow, the normal structure of bone marrow is destroyed and replaced by tumor cell components with a higher density, and the extracellular space becomes narrowed. Therefore, compared with benign lesions such as hemangioma, the diffusion ability of water molecules in vertebral metastases is limited, and the IVIM-DWI image presents a high signal intensity, and the standard ADC value and *D* value are correspondingly reduced. Some studies have also verified the results of this conclusion [39, 40]. If the lesion contains osteoblastic components in which water content is limited, the standard ADC value and *D* value will also be affected [41, 42]. Therefore, further research is needed. In this study, the differential diagnostic efficiency of *D* value

was significantly higher, indicating *D* value was more effective in the differential diagnosis of vertebral metastases and VHs.

However, *f* value and *D** value related to perfusion parameters had no statistical differences between the two vertebral lesions in our research. In some previous studies, *f* value increased due to the high vascularization and abundant blood supply in neoplastic lesions [43–45]. In our study, *f* value has declined. We speculate that the reason may be due to the abundant but not mature neovascularization in malignant lesions, and the relatively high vascular permeability may lead to early perfusion, rapid progress and short duration [46]. Besides, the *f* value may also be affected by different sources of metastases. *D** value usually represents the blood flow velocity corresponding to perfusion. Our results are consistent with the most studies [40, 42], suggesting that *D** may be not meaningful for the differential diagnosis for two vertebral lesions [47]. The stability and repeatability of the above results still need to be further verified by subsequent studies.

This study had several limitations. First, the overall sample size was small. Big data may provide more precise diagnostic value. Second, quantitative comparisons were performed using the mean value of manually drawn ROIs, which may make the analysis prone to error.

In conclusion, FOCUS IVIM-DWI can quantitatively differentiate atypical VHs from vertebral metastases. It may become an important imaging technique to reflect the metabolic activity of lesions and improve diagnostic accuracy.

## Compliance with ethical standards

**Conflict of interest** The authors declare that they have no conflict of interest.

## References


1. Porter BA, Shields AF, Olson DO (1986) Magnetic resonance imaging of bone marrow disorders. Radiol Clin North Am 24(2):269–289
2. McEvoy SH, Farrell M, Brett F, Looby S (2016) Haemangioma, an uncommon cause of an extradural or intradural extramedullary mass: case series with radiological pathological correlation. Insights Imaging 7(1):87–98. https://doi.org/10.1007/s13244-015-0432-y
3. Murphey MD, Fairbairn KJ, Parman LM, Baxter KG, Parsa MB, Smith WS (1995) From the archives of the AFIP. Musculoskeletal angiomatous lesions: radiologic-pathologic correlation. Radiographics 15(4):893–917. https://doi.org/10.1148/radiographics.15.4.7569134
4. Morales KA, Arevalo-Perez J, Peck KK, Holodny AI, Lis E, Karimi S (2018) Differentiating atypical hemangiomas and metastatic vertebral lesions: the role of T1-weighted dynamic contrast-enhanced MRI. AJNR Am J Neuroradiol 39(5):968–973. https://doi.org/10.3174/ajnr.A5630
5. Bender YY, Boker SM, Diederichs G, Walter T, Wagner M, Fallenberg E, Liebig T, Rickert M, Hamm B, Makowski MR (2017) MRI for the detection of calcific features of vertebral haemangioma. Clin Radiol 72(8):692.e1-692.e7. https://doi.org/10.1016/j.crad.2017.02.018
6. Nigro L, Donnarumma P (2017) Vertebral hemangiomas: common lesions with still many unknown aspects. J Spine Surg 3(2):309–311. https://doi.org/10.21037/jss.2017.05.11
7. Leeds NE, Kumar AJ, Zhou XJ, McKinnon GC (2000) Magnetic resonance imaging of benign spinal lesions simulating metastasis: role of diffusion-weighted imaging. Top Magn Reson Imaging 11(4):224–234
8. Erlemann R (2006) Imaging and differential diagnosis of primary bone tumors and tumor-like lesions of the spine. Eur J Radiol 58(1):48–67. https://doi.org/10.1016/j.ejrad.2005.12.006
9. Zajick DC Jr, Morrison WB, Schweitzer ME, Parellada JA, Carrino JA (2005) Benign and malignant processes: normal values and differentiation with chemical shift MR imaging in vertebral marrow. Radiology 237(2):590–596. https://doi.org/10.1148/radiol.2372040990
10. Suh CH, Yun SJ, Jin W, Lee SH, Park SY, Ryu CW (2018) ADC as a useful diagnostic tool for differentiating benign and malignant vertebral bone marrow lesions and compression fractures: a systematic review and meta-analysis. Eur Radiol 28(7):2890–2902. https://doi.org/10.1007/s00330-018-5330-5
11. Le Bihan D, Breton E, Lallemand D, Aubin ML, Vignaud J, Laval-Jeantet M (1988) Separation of diffusion and perfusion in intravoxel incoherent motion MR imaging. Radiology 168(2):497–505. https://doi.org/10.1148/radiology.168.2.3393671
12. Joo I, Lee JM, Han JK, Choi BI (2014) Intravoxel incoherent motion diffusion-weighted MR imaging for monitoring the therapeutic efficacy of the vascular disrupting agent CKD-516 in rabbit VX2 liver tumors. Radiology 272(2):417–426. https://doi.org/10.1148/radiol.14131165
13. Park S, Yoon JK, Chung NS, Kim SH, Hwang J, Lee HY, Kwack KS (2018) Correlations between intravoxel incoherent motion diffusion-weighted MR imaging parameters and (18)F-FDG PET/CT metabolic parameters in patients with vertebral bone metastases: initial experience. Br J Radiol 91(1086):20170889. https://doi.org/10.1259/bjr.20170889
14. Luciani A, Vignaud A, Cavet M, Nhieu JT, Mallat A, Ruel L, Laurent A, Deux JF, Brugieres P, Rahmouni A (2008) Liver cirrhosis: intravoxel incoherent motion MR imaging–pilot study. Radiology 249(3):891–899. https://doi.org/10.1148/radiol.2493080080
15. Le Bihan D (2008) Intravoxel incoherent motion perfusion MR imaging: a wake-up call. Radiology 249(3):748–752. https://doi.org/10.1148/radiol.2493081301
16. Liu C, Liang C, Liu Z, Zhang S, Huang B (2013) Intravoxel incoherent motion (IVIM) in evaluation of breast lesions: comparison with conventional DWI. Eur J Radiol 82(12):e782-789. https://doi.org/10.1016/j.ejrad.2013.08.006
17. Le Bihan D, Breton E, Lallemand D, Grenier P, Cabanis E, Laval-Jeantet M (1986) MR imaging of intravoxel incoherent motions: application to diffusion and perfusion in neurologic disorders. Radiology 161(2):401–407. https://doi.org/10.1148/radiology.161.2.3763909
18. Henkelman RM (1990) Does IVIM measure classical perfusion? Magn Reson Med 16(3):470–475. https://doi.org/10.1002/mrm.1910160313
19. Le Bihan D, Turner R (1992) The capillary network: a link between IVIM and classical perfusion. Magn Reson Med 27(1):171–178. https://doi.org/10.1002/mrm.1910270116
20. Lemke A, Laun FB, Simon D, Stieltjes B, Schad LR (2010) An in vivo verification of the intravoxel incoherent motion effect in diffusion-weighted imaging of the abdomen. Magn Reson Med 64(6):1580–1585. https://doi.org/10.1002/mrm.22565

21. Notohamiprodjo M, Chandarana H, Mikheev A, Rusinek H, Grinstead J, Feiweier T, Raya JG, Lee VS, Sigmund EE (2015) Combined intravoxel incoherent motion and diffusion tensor imaging of renal diffusion and flow anisotropy. Magn Reson Med 73(4):1526–1532. https://doi.org/10.1002/mrm.25245
22. Saritas EU, Cunningham CH, Lee JH, Han ET, Nishimura DG (2008) DWI of the spinal cord with reduced FOV single-shot EPI. Magn Reson Med 60(2):468–473. https://doi.org/10.1002/mrm.21640
23. Karampinos DC, Ruschke S, Dieckmeyer M, Diefenbach M, Franz D, Gersing AS, Krug R, Baum T (2018) Quantitative MRI and spectroscopy of bone marrow. J Magn Reson Imaging 47(2):332–353. https://doi.org/10.1002/jmri.25769
24. Singhal V, Bredella MA (2019) Marrow adipose tissue imaging in humans. Bone 118:69–76. https://doi.org/10.1016/j.bone.2018.01.009
25. Hajalioghli P, Daghighi MH, Ghaffari J, Mirza-Aghazadeh-Attari M, Khamanian J, Ghaderi P, Yazdaninia I, Daghighi S, Zarrintan A (2020) Accuracy of diffusion-weighted imaging in discriminating atypical vertebral haemangiomas from malignant masses in patients with vertebral lesions: a cross-sectional study. Pol J Radiol 85:e340–e347. https://doi.org/10.5114/pjr.2020.97602
26. Geith T, Schmidt G, Biffar A, Dietrich O, Durr HR, Reiser M, Baur-Melnyk A (2012) Comparison of qualitative and quantitative evaluation of diffusion-weighted MRI and chemical-shift imaging in the differentiation of benign and malignant vertebral body fractures. AJR Am J Roentgenol 199(5):1083–1092. https://doi.org/10.2214/AJR.11.8010
27. Zheng S, Dong Y, Miao Y, Liu A, Zhang X, Wang B, Ge Y, Liu Y, Wang S (2014) Differentiation of osteolytic metastases and Schmorl's nodes in cancer patients using dual-energy CT: advantage of spectral CT imaging. Eur J Radiol 83(7):1216–1221. https://doi.org/10.1016/j.ejrad.2014.02.003
28. Mannelli L, Monti S, Corrias G, Fung MM, Nyman C, Golia Pernicka JS, Do RKG (2019) Comparison of navigator triggering reduced field of view and large field of view diffusion-weighted imaging of the pancreas. J Comput Assist Tomogr 43(1):143–148. https://doi.org/10.1097/RCT.0000000000000778
29. Dong H, Li Y, Li H, Wang B, Hu B (2014) Study of the reduced field-of-view diffusion-weighted imaging of the breast. Clin Breast Cancer 14(4):265–271. https://doi.org/10.1016/j.clbc.2013.12.001
30. Singer L, Wilmes LJ, Saritas EU, Shankaranarayanan A, Proctor E, Wisner DJ, Chang B, Joe BN, Nishimura DG, Hylton NM (2012) High-resolution diffusion-weighted magnetic resonance imaging in patients with locally advanced breast cancer. Acad Radiol 19(5):526–534. https://doi.org/10.1016/j.acra.2011.11.003
31. Feng Z, Min X, Sah VK, Li L, Cai J, Deng M, Wang L (2015) Comparison of field-of-view (FOV) optimized and constrained undistorted single shot (FOCUS) with conventional DWI for the evaluation of prostate cancer. Clin Imaging 39(5):851–855. https://doi.org/10.1016/j.clinimag.2015.03.004
32. Lasbleiz J, Le Ster C, Guillin R, Saint-Jalmes H, Gambarota G (2019) Measurements of diffusion and perfusion in vertebral bone marrow using intravoxel incoherent motion (IVIM) with multishot, readout-segmented (RESOLVE) echo-planar imaging. J Magn Reson Imaging 49(3):768–776. https://doi.org/10.1002/jmri.26270
33. Dietrich O, Geith T, Reiser MF, Baur-Melnyk A (2017) Diffusion imaging of the vertebral bone marrow. NMR Biomed. https://doi.org/10.1002/nbm.3333
34. Koutoulidis V, Papanikolaou N, Moulopoulos LA (2018) Functional and molecular MRI of the bone marrow in multiple myeloma. Br J Radiol 91(1088):20170389. https://doi.org/10.1259/bjr.20170389
35. Park HJ, Lee SY, Rho MH, Chung EC, Kim MS, Kwon HJ, Youn IY (2016) Single-shot echo-planar diffusion-weighted MR imaging at 3T and 1.5T for differentiation of benign vertebral fracture edema and tumor infiltration. Korean J Radiol 17(5):590–597. https://doi.org/10.3348/kjr.2016.17.5.590
36. Iima M, Le Bihan D (2016) Clinical intravoxel incoherent motion and diffusion MR imaging: past, present, and future. Radiology 278(1):13–32. https://doi.org/10.1148/radiol.2015150244
37. Park S, Kwack KS, Chung NS, Hwang J, Lee HY, Kim JH (2017) Intravoxel incoherent motion diffusion-weighted magnetic resonance imaging of focal vertebral bone marrow lesions: initial experience of the differentiation of nodular hyperplastic hematopoietic bone marrow from malignant lesions. Skelet Radiol 46(5):675–683. https://doi.org/10.1007/s00256-017-2603-z
38. Winfield JM, Poillucci G, Blackledge MD, Collins DJ, Shah V, Tunariu N, Kaiser MF, Messiou C (2018) Apparent diffusion coefficient of vertebral haemangiomas allows differentiation from malignant focal deposits in whole-body diffusion-weighted MRI. Eur Radiol 28(4):1687–1691. https://doi.org/10.1007/s00330-017-5079-2
39. Pozzi G, Albano D, Messina C, Angileri SA, Al-Mnayyis A, Galbusera F, Luzzati A, Perrucchini G, Scotto G, Parafioriti A, Zerbi A, Sconfienza LM (2018) Solid bone tumors of the spine: diagnostic performance of apparent diffusion coefficient measured using diffusion-weighted MRI using histology as a reference standard. J Magn Reson Imaging 47(4):1034–1042. https://doi.org/10.1002/jmri.25826
40. Lim HK, Jee WH, Jung JY, Paek MY, Kim I, Jung CK, Chung YG (2018) Intravoxel incoherent motion diffusion-weighted MR imaging for differentiation of benign and malignant musculoskeletal tumours at 3 T. Br J Radiol 91(1082):20170636. https://doi.org/10.1259/bjr.20170636
41. Hacklander T, Scharwachter C, Golz R, Mertens H (2006) Value of diffusion-weighted imaging for diagnosing vertebral metastases due to prostate cancer in comparison to other primary tumors. Rofo 178(4):416–424. https://doi.org/10.1055/s-2006-926566
42. Baik JS, Jung JY, Jee WH, Chun CW, Kim SK, Shin SH, Chung YG, Jung CK, Kannengiesser S, Sohn Y (2017) Differentiation of focal indeterminate marrow abnormalities with multiparametric MRI. J Magn Reson Imaging 46(1):49–60. https://doi.org/10.1002/jmri.25536
43. Noij DP, Martens RM, Marcus JT, de Bree R, Leemans CR, Castelijns JA, de Jong MC, de Graaf P (2017) Intravoxel incoherent motion magnetic resonance imaging in head and neck cancer: a systematic review of the diagnostic and prognostic value. Oral Oncol 68:81–91. https://doi.org/10.1016/j.oraloncology.2017.03.016
44. Guiu B, Petit JM, Capitan V, Aho S, Masson D, Lefevre PH, Favelier S, Loffroy R, Verges B, Hillon P, Krause D, Cercueil JP (2012) Intravoxel incoherent motion diffusion-weighted imaging in nonalcoholic fatty liver disease: a 3.0-T MR study. Radiology 265(1):96–103. https://doi.org/10.1148/radiol.12112478
45. Kang KM, Lee JM, Yoon JH, Kiefer B, Han JK, Choi BI (2014) Intravoxel incoherent motion diffusion-weighted MR imaging for characterization of focal pancreatic lesions. Radiology 270(2):444–453. https://doi.org/10.1148/radiol.13122712
46. Federau C (2017) Intravoxel incoherent motion MRI as a means to measure in vivo perfusion: a review of the evidence. NMR Biomed. https://doi.org/10.1002/nbm.3780
47. Lee JH, Cheong H, Lee SS, Lee CK, Sung YS, Huh JW, Song JA, Choe H (2016) Perfusion assessment using intravoxel incoherent motion-based analysis of diffusion-weighted magnetic resonance imaging: validation through phantom experiments. Investig Radiol 51(8):520–528. https://doi.org/10.1097/RLI.0000000000000262